# Fabrication and characterization of low pressure micro-resistojets with integrated heater and temperature measurement

Guerrieri, Dadui C.; Silva, Marsil A.C.; Van Zeijl, Henk; Cervone, Angelo; Gill, Eberhard

**DOI**
10.1088/1361-6439/aa90fb

**Publication date**
2017

**Document Version**
Accepted author manuscript

**Published in**
Journal of Micromechanics and Microengineering

# Fabrication and Characterization of Low Pressure Micro-Resistojets with Integrated Heater and Temperature Measurement

**Daduí C. Guerrieri[1], Marsil A. C. Silva[1], Henk van Zeijl[2], Angelo Cervone[1], Eberhard Gill[1]**

[1] Space Engineering, Faculty of Aerospace Engineering, TU Delft, The Netherlands
[2] Else Kooi Laboratory, TU Delft, The Netherlands

E-mail: d.cordeiroguerrieri@tudelft.nl

**Abstract.** Three Low Pressure Micro-resistojets (LPM) with integrated heater and temperature measurement were designed, manufactured and characterized at Delft University of Technology. The devices were manufactured using Silicon-based Micro Electro Mechanical Systems (MEMS) technology including a heater made of Molybdenum for better operations at high temperature. The resistace of the heaters is used to estimate the chip temperature giving them a double function as heater and sensor simultaneously. The manufacturing steps are described in detail. A special interface was manufactured to hold the MEMS device considering the mechanical and electrical aspects. The MEMS devices are characterized for three different aspects: mechanical, electrical and propulsion. The three designed devices were tested mechanically and electrically, and one design was tested in terms of propulsion performance in a near-operational condition. The tests are promising and open the path to design a flight demonstration model.

## 1. Introduction

The ongoing worldwide trend towards the miniaturization of systems is also found in the space sector, where the satellites are getting even smaller in terms of mass and volume. Nano- and pico-satellites are restricted in terms of subsystem requirements, for instance, regarding the power consumption, the use of hazardous materials, internal pressure, size and mass constraints. It is therefore an engineering challenge to implement a propulsion system for those satellites. Even though several micro-propulsion devices have already been proposed, there are still gaps in the performance range. A proper design of such propulsion systems will increase the capabilities of those very small satellites allowing functionalities such as to perform an orbit transfer, station keeping of constellations, and formation flying [1].

One of the propulsion alternatives for very small satellites is the Low Pressure Micro-Resistojet (LPM), also known as Free Molecule Micro-Resistojet (FMMR), that is based on rarefied gas dynamics. The propellant particles are heated and expanded at high Knudsen number to a high exhaust velocity through the grid of channels or slots. It has been proposed first in the late 1990s [2]. In 2000s a different design was presented based on a double-sided polished silicon wafer using the MEMS technology [3]. Thus design is based on a heater chip with a flat plate geometry of 19.2 $\times$ 19.2 mm$^2$ $\times$ 500 $\mu$m thickness that contains 44 expansion

slots with dimensions of 100 $\mu$m wide by 5.375 mm long. Helium, Nitrogen, Argon, and Carbon dioxide were tested as propellant. The delivered thrust was from 0.1 to 1.6 mN for mass flow rates from 25 to 100 sccm depending on the propellant. The specific impulse was from 40 to 140 for heater chip temperatures raging from 325 to 525 K and depending on the propellant. In 2013, Palmer et al. [4] fabricated and tested a different design with thick silicon dioxide insulation and suspension to reduce the heat lost improving the thruster efficiency. They showed that it is possible to keep the temperature at about 270°C in the heated island walls, while the surrounding silicon is about 50°C.

Cervone et al. [5] present a complete conceptual design of the LPM system based on a sublimating solid propellant. The tank works under sublimation conditions at low pressure, the propellant vapour goes through a plenum and is expelled through heater chip slots to outer space, producing thrust. They also proposed an optimized expansion slot of 200 $\mu$m $\times$ 500 $\mu$m with 15° divergence angle for the last half of the expansion slot length. Guerrieri et al. [6] published a sensitivity analysis on the expansion slot (or channel) cross-section geometry of the heater chip using a numerical simulation. The optimized microchannel is composed by the first-half as divergent channel, and the second-half as straight channel. The first-half is used to increase the mass flow rate and the second to increase the heat transfer and the propellant temperature. They showed that selecting a proper geometry, the thrust can increase up to 480% while the specific impulse decreases by 5%, and the power consumption decreases by 67%.

The LPM is still in a maturation phase, and there are still some issues to be solved before the development of a flight demonstration model. However, it is presented in this paper the first LPM developed by TU Delft in order to meet the strict requirements of nano- and pico-satellites. The advantage of this propulsion system is the low needed power consumption and the very low internal pressure, besides the usage of green propellants such as water. Water as propellant has been proved to be an interesting choice for micro-resistojets as it provides a very high $\Delta v$ per volume of propellant when compared to other green propellants [7]. Nevertheless, the propellant used in this paper in order to characterize the thruster was Nitrogen because it is cheap, easy to handle, and a well-known propellant used for this propose [3, 4, 6]. The heater chip based on silicon wafer is composed of a grid of holes/slots and a heater made out of Molybdenum (Mo). The Mo presents a linear resistivity response to the temperature up to 700°C [8]. This capability was used to control the heater chip temperature during the propulsion test when required high temperature through the proportional-integral-derivative (PID) controller. In addition, a special interface was designed and built to hold the heater chip combining fluidic, electric and mechanic connections.

## 2. Analytical Models

### *2.1. LPM theory*

This specific propulsion system was designed to work in a transition flow regime. This regime is defined by a Knudsen number $Kn$ between 0.1 and 10. $Kn$ defines the degree of gas rarefaction which depends on the average distance travelled by the molecules between collisions,

$$Kn = \frac{\lambda}{L} \tag{1}$$

where $\lambda$ is the molecular mean free path, and $L$ is the characteristic dimension. Under these rarefied gas dynamic conditions the ideal gas equation and the Maxwell theory can be applied as described [3]. For the mass flow rate $\dot{m}$

$$\dot{m} = \alpha P_0 \sqrt{\frac{m}{2\pi k T_0}} A_e \tag{2}$$

where $P_0$ is the plenum pressure, $m$ is the mass of propellant molecules, $k$ the Boltzmann constant, $T_0$ the plenum temperature, $A_e$ the exit area, and $\alpha$ the transmission coefficient. The transmission coefficient is the actual mass flow rate to the mass flow rate in the free molecular limit ratio, i.e. for an infinitely thin channel, the transmission coefficient is equal to 1. Its value depends on the geometry. For instance, in a cylindrical channel with an aspect ratio of 5 the transmission coefficient is 0.19, in a slot with an aspect ratio of 5 is 0.38, and in a slot with an aspect ratio of 2.5 it is 0.49 [9]. The exit velocity is given by

$$u_e = \sqrt{\frac{\pi k T_w}{2m}} \tag{3}$$

where $T_w$ is the wall temperature. Finally, for those propulsion systems, according to Ketsdever et al. [3], the thrust can be written as

$$\Im = \dot{m} u_e = \frac{\alpha P_0 A_e}{2} \sqrt{\frac{T_w}{T_0}} \tag{4}$$

and the specific impulse as

$$I_{sp} = \frac{\Im}{\dot{m} g_0} = \sqrt{\frac{\pi k T_w}{2 m g_0^2}} \tag{5}$$

*2.2. Electro-thermal theory*

The material and the geometry play a major role in the performance of the resistors. This can be mathematically seen in the following equation:

$$R_0 = \frac{\rho L}{A_R} \tag{6}$$

where $R_0$ is the resistance measured at room temperature $T_0$, $\rho$ is the material resistivity, $L$ is the length and $A_R$ the cross-sectional area of the specimen. Another important relation is between the resistance and the temperature, expressed as

$$\beta = \frac{R - R_0}{R_0 \left(T - T_0\right)} \tag{7}$$

where $\beta$ is the temperature coefficient of the resistance, and $R$ is the resistance measured at temperature $T$. Even though the value of $\beta$ is basically related to the material, it is good practice to characterize its value for each device as any impurities induced by the manufacturing process can affect this value. A complete characterization of a similar device has been performed by [8].

## 3. Design Description

The heater chip is the main part of the LPM, manufactured using MEMS processing techniques. Three different slot geometries are considered for the design: a grid of 40×40 microchannels with a diameter of 100 $\mu$m, a grid of 1×10 large slots with a width of 200 $\mu$m and length of 8 mm, and a grid of 1×20 small slots with a width of 100 $\mu$m and length of 8 mm. Those devices are designed to have the same exit area of 16 mm$^2$ and the same design resistance. Figure 1 shows the mask for the grid of holes (GH), the grid of large slots (GLS), the grid of small slots (GSS), and the resistance.

As shown in Figure 1, the heater is composed by 38 resistances arranged into two sets of 19 resistances in parallel, with these two sets arranged in series. Each resistance was designed to have length of 100 mm, width of 20 $\mu$m, and thickness of 200 $n$m. Considering a material

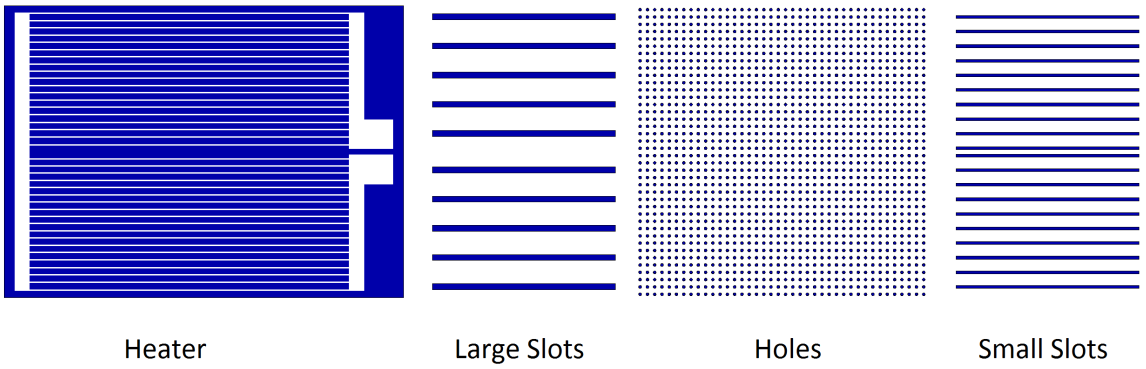


**Figure 1.** Masks used in the manufacturing process of the devices. The same heater mask was used in all devices, namely GLS, GH and GSS chips.

resistivity of 400 $n\Omega$/m for Mo [8], the total design resistance is 105 Ω. It was designed to produce 1.4 W of power given a voltage of 12 V.

Assuming Nitrogen as propellant, a range of plenum pressures from 50 to 300 Pa, and a heater chip temperature from 300 to 600 K, each type of device has different range of mass flow rate and thrust. For the GH the range of mass flow rate is from 0.2 to 1.0 mg/s and the range of thrust is from 0.1 to 0.5 mN, for the GLS they are from 0.4 to 2.5 mg/s and from 0.2 to 1.3 mN, and for the GSS they from 0.3 to 2.0 mg/s and from 0.1 to 1.0 mN. The specific impulse has the same range in all devices from 51 to 72 s.

## 4. Description of Manufacturing Process

The used silicon wafer was a double side polished with thickness of 500 $\mu$m. First, lithographic alignment marks are etched on the wafer surface to enable high accuracy alignment of subsequent layers. A layer of 500 $n$m of LPCVD (Low Pressure Chemical Vapour Deposition) silicon nitride was deposited to make the isolation between the wafer and the resistance, see Figure 2-a. A layer of 200 $n$m of Mo was deposited over the layer of silicon nitride by sputtering. A layer of 300 $n$m of PECVD TEOS (Plasma-Enhanced Chemical Vapour Deposition Tetraethoxysilane) was deposited to make the hard mask for Mo, see Figure 2-b. The heater mask (left side of Figure 1) was made by photoresist, see Figure 2-c. The TEOS (hard-mask) was etched with buffered hydrofluoric acid (BHF), and then the Mo was also etched with aluminum etch at 35°C, both processes were a wet etching, see Figure 2-d. To complete this step of the process, the photoresist was stripped off with plasma, and the TEOS was removed with BHF, see Figure 2-e.

To etch through the wafer, it is necessary to have the hard-mask layer on one side, and a stopping layer on another side. On both sides a layer of 5 $\mu$m of silicon dioxide was deposed, see Figure 2-f. On the hard-mask the photoresist to make the soft-mask was also deposed, see Figure 2-g. Figure 1 shows the three masks used for the GH, GLS, and GSS; each of these masks was used on one wafer, producing three different wafers. The soft-mask was used to etch the hard-mask (silicon dioxide) and the silicon nitride with plasma etching, see Figure 2-h. And finally, the soft- and hard-mask were used to etch the silicon by anisotropic Deep Reactive Ion Etching (DRIE), see Figure 2-i. Then, cleaning and removal of the soft-mask, hard-mask and stopping layers were done. Figure 2-j shows the schematic cross-section of the device after the manufacturing process. Finally, the wafers were diced as shown in Figure 3. As it is possible to see, 16 thruster devices of same design were made using one single wafer.

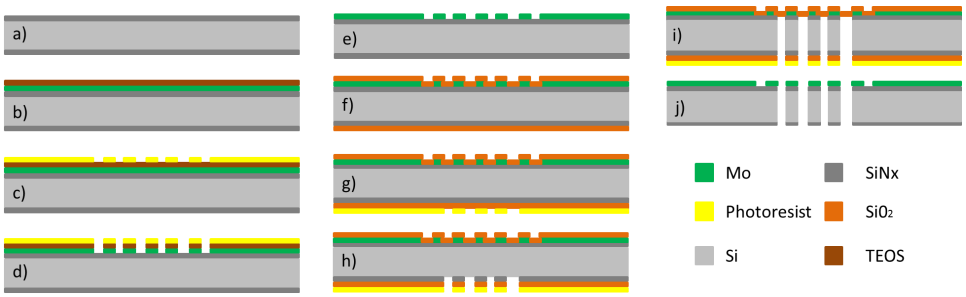


**Figure 2.** Schematic cross section of heater chip during the steps of the manufacturing process.

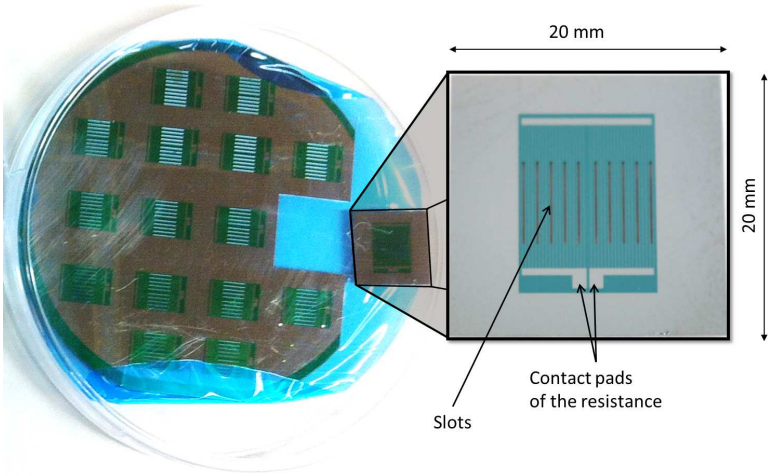


**Figure 3.** Wafer with large slots chips (GLS) after manufacturing and dicing process.

## 5. Experimental Description

In total, three wafers were processed, each one with a specific design (GLS, GH, GSS). The heater chips were characterized in terms of mechanical, electrical and propulsion aspects. For this reason a special interface was designed and built to provide the mechanical and electrical interface, see Figure 4. It is made of teflon and aluminium, with teflon providing good isolation that supports a moderately high temperature and aluminium sufficient structure strength.

### *5.1. Mechanical Characterization*

A sample of manufactured device was measured in order to compare the actual dimensions to the design ones. An optical microscope was used for the main dimensions, and an electron microscope for small details. According to the proposed design, the GH has a hole diameter of 100 $\mu$m and a pitch of 200 $\mu$m, the GLS has width of 200 $\mu$m and length of 6.28 mm, the GSS has width of 100 $\mu$m and length of 6.28 mm, and the resistance the width of 20 $\mu$m and the length of 11 mm.

### *5.2. Eletrical Characterization*

The devices' resistances were measured at room temperature in order to compare them to the design ones. In addition, a test bench using a thermal camera with 5% accuracy of reading and a power supply was set up to characterize the temperature coefficient of the resistance ($\beta$). The experimental setup and a sequence of images taken with the infrared camera from the backside of the GLS heater chip is shown in Figure 5. These measurements are used to estimate the average

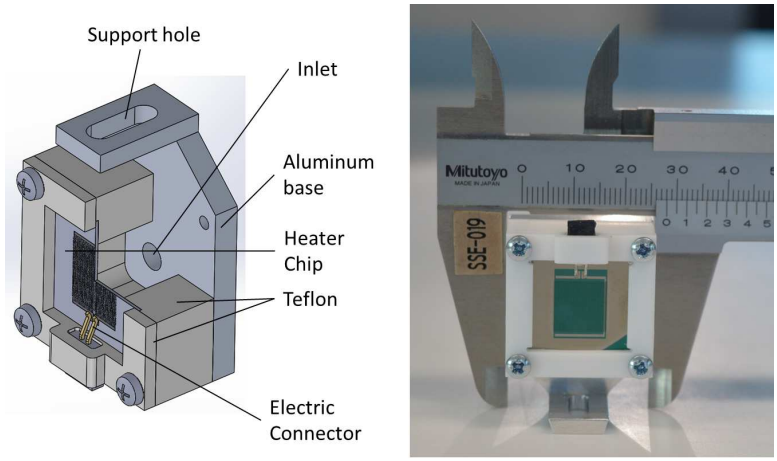


**Figure 4.** Left: sketch of the interface prototype of the thruster. Right: picture of the actual assembled prototype.

temperature of the heater chip over time. It is performed by applying a constant voltage to the heaters in order to measure the resistance. Then, $\beta$ can be estimated using Equation 7.

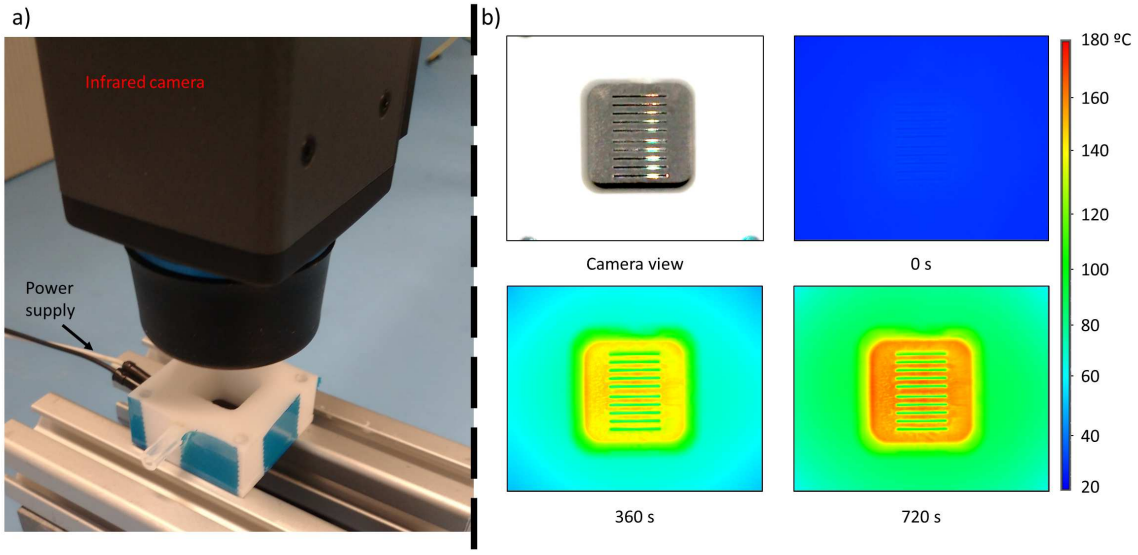


**Figure 5.** a) Setup used to perform the experiment in order to define the temperature coefficient of the resistance ($\beta$) in Equation 7. b) The temperature measurement of the chip surface using an infrared camera. The left top side shows the camera view; the chip is painted with graphite ink that provides an uniform emissivity of 0.97. The other images are from the infrared camera at different moments after applying a constant voltage of 39 V.

*5.3. Propulsion characterization*

A test bench using a pendulum was used to measure the thrust. Figure 6 shows a simplified piping and instrumentation diagram of the test bench, and the Table 1 presents the features of the sensors. The propellent is stored in a tank outside the vacuum chamber and is fed through a flexible tube attached to the rotation point of the pendulum in order to reduce disturbances

produced by the flow of gas inside the tube. A valve is used to regulate the plenum pressure and to operate the thruster during the tests. A capacitive sensor is placed behind the pendulum to measure its displacement.

The method using the pendulum presents an error due to the calibration process of about 13 $\mu$N, as described in detail in [10, 11]. The experiment was performed in a vacuum oven under different background pressures ranging from 15 to 35 Pa and different heater chip temperature: room temperature 24°C; and high temperature 149°C.

Using the results obtained from the electrical characterization, the resistor on the chip was used as a double function heater and temperature sensor. Based on the voltage and current measurements a PID controller was used to control the heater chip temperature during the high temperature experiment. This temperature sensor was characterized for a temperature range from 20 to 160 °C with a accuracy of 8 °C due to the noise given mainly by the power supply.

In order to have a low pressure inside the plenum, the valve (FC-01) is controlled by Pulse-Width Modulation (PWM). Thus, the mass flow rate depends on the tank pressure (PT-01), tank temperature (TT-01) and the PWM signal. When the valve is opened the propellant is expelled into the vacuum chamber increasing the background pressure quickly. Due to this, the only considered measurement for this paper are the data just after the valve opening.

To make sure that the background pressure is the same in all measurements, an automatic control of the experiment was implemented. When the pressure sensor (PT-02) measures the desired background pressure, a command is sent to the valve (FC-01) starting the thrust. When the vacuum chamber reaches a pressure of 5 Pa higher than the desired background pressure, a new command is sent, closing the valve. Then, the cycle starts again.

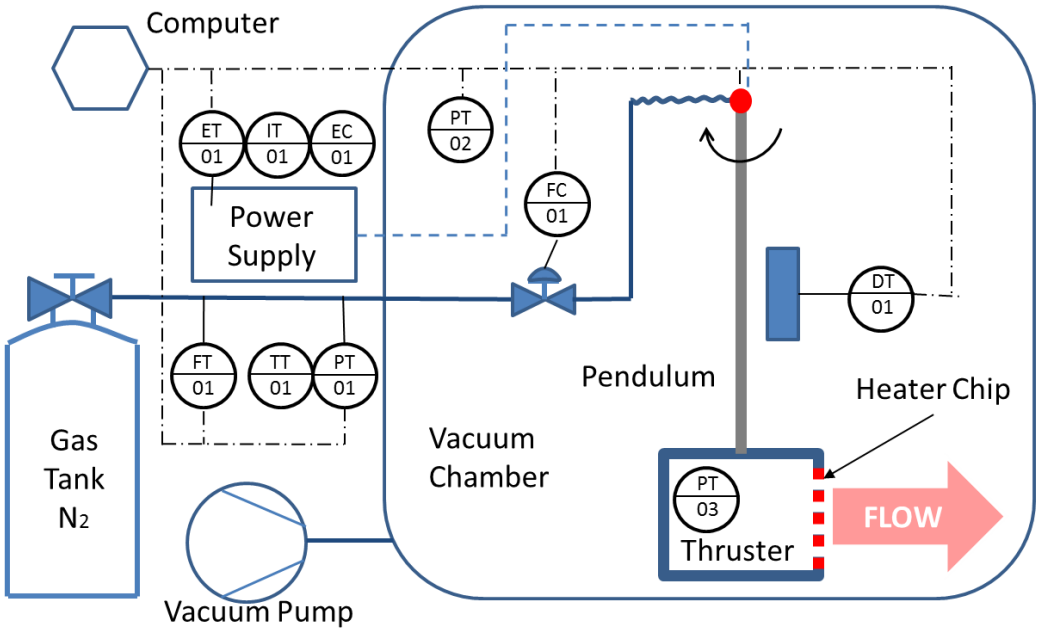


**Figure 6.** A simplified piping and instrumentation diagram of the test bench.

The pendulum is an indirect measurement of the thrust and needs to be calibrated before each test. The pendulum is calibrated using a known force generated by a coil and the displacement, measured from DT-01, is recorded. This calibration defines the linear relationship between

**Table 1.** The features of the sensors and actuators.

| # | Sensors/Actuators | Manufacturer number | Operation range | Accuracy |
|---|---|---|---|---|
| DT-01 | Displacement | DT6220 - CS05 (Micro-Epsilon) | 0 - 0.5 mm | ± 40 nm |
| ET-01 | Voltage | SM7020 | 0 - 70 V | ± 70 mV |
| IT-01 | Current | (Delta Elektronika BV) | 0 - 20 A | ± 20 mA |
| FT-01 | Flow | 5850S (Brooks) | 0 - 2 ln/min N2 | ± 2 mln/min |
| PT-01 | Pressure | MS5803-05BA | 0 - 5 bar | ± 1.5 mbar |
| TT-01 | Temperature | (TE connectivity) | -40 - 80 °C | ± 2.5 °C |
| PT-02 | Pressure | VSP 3000 (Vacuubrand) | 0.001 - 1000 mbar | ± 15% of displayed value |
| PT-03 | Pressure | HCLA12X5DU (First sensor) | 0 - 12.5 mbar | ± 0.016 mbar |

displacement and force, more details can be found in [10, 11]. This relation is used to calculate the thrust based on the measured displacement. During the experiment, the measurements from all sensors showed in Figure 6 were recorded. The propellant used to perform the test was Nitrogen because it is commonly used in the literature besides of being cheap and easy to handle.

## 6. Results and Discussion

The results of the three characterizations (mechanical, electrical, and propulsion) are presented and discussed in this section.

### *6.1. Mechanical Characterization*

The design dimensions given in Subsection 5.1 were compared to the measured values shown in Figure 7. It is possible to see a slight difference between the design and manufactured. The most relevant difference is that there is a layer of silicon nitride in the stop layer side that was not etched equally compared to the silicon wafer, giving a small protuberance of about 3 $\mu$m as seen in Figure 8. The same difference can be seen in Figure 7 through the measurements made in the GH chip: the measured hole in the silicon wafer is 106.3 $\mu$m while in the silicon nitride layer is 100.7 $\mu$m. Figure 8 also shows that the roughness in the wall which might affect the thruster performance. Another relevant difference is related to the thickness of the Mo layer, where lesser Mo then expected was deposed, resulting in a higher resistivity as it is showed in Subsection 6.2. This affects the amount of voltage necessary to be applied to achieve the expected power.

### *6.2. Electrical Characterization*

As commented previously the resistances of the devices are higher than designed. The GLS and GSS present, respectively, an average resistance of 272.76 ± 8.18 Ω and 263.40 ± 7.85 Ω, around 2.5 times larger than expected. The GH, that was processed at a different moment, presents an average resistance of 435.13 ± 31.96 Ω, around 4 times larger than expected. This increased resistance results in a higher voltage to achieve the required power, however this is not an issue for the tests presented here.

The temperature, as measured using the thermal camera is plotted against the resistance measured for each device and showed in Figure 9. Those measured values were used to estimate $\beta$ in order to measure the temperature according to the heater chip resistivity. The average value

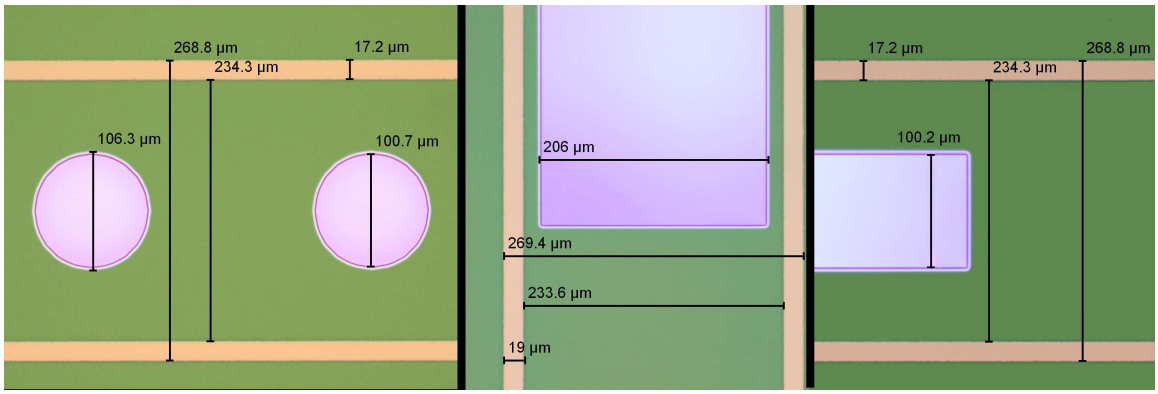


**Figure 7.** Dimensions of the chip geometries measured using an optical microscope with 10× magnification. On the left side the GH, in the center the GLS and on the right side the GSS.

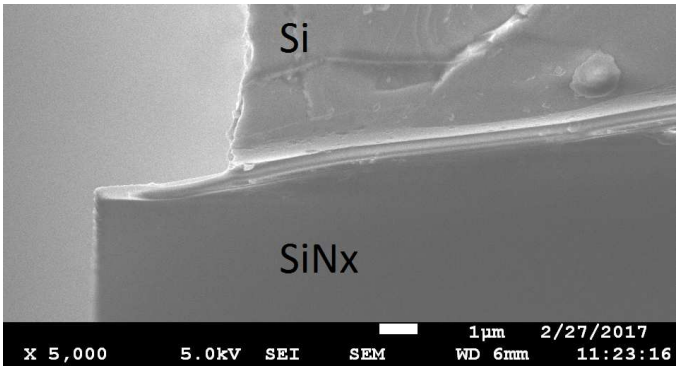


**Figure 8.** Cross-sectional view of the GLS chip using a scanning electron microscope.

of $\beta$ for the three tested heater chip is $0.0015°C^{-1}$ and the standard deviation is $8.63\times10^{-5}°C^{-1}$. Figure 10 presents the comparison between the measurements with the thermal camera and the estimation done with Equation 7 for the GSS, GH and GLS. As it is possible to see they match quite well, proving that using the resistivity method gives an acceptable temperature estimation. This approach is useful to control the temperature of the thruster with no addition of electronic component such as thermocouple or similar, making this propulsion system even more suitable for use in very small satellites.

*6.3. Propulsion Characterization*

The thrust was characterized performing tests using the pendulum as described in section 5. The tests were performed using the GLS chip which provides higher thrust with the same plenum pressure due to its geometry. Due to the background pressure, it was decided to perform the tests with the plenum pressure between 200 and 280 Pa. The minimum pressure 200 Pa is chosen because the background pressure represents less than 10% of the plenum pressure. The maximum pressure 280 Pa has been selected because it represents the boundary between the transitional regime and the slip flow regime by meaning a Knudsen number of 0.1. Thus, the tests using high temperatures were performed under slip flow regime. This happened because the plenum temperature increases due to the high heater chip temperature with a consequent increase in plenum pressure. The range of mass flow rates was kept between 2.2 and 3.6 mg/s. A carefully comparison between both scenarios has to be done in order to assess the differences the two regimes. However, such comparison is out of the scope of this paper that is dedicated

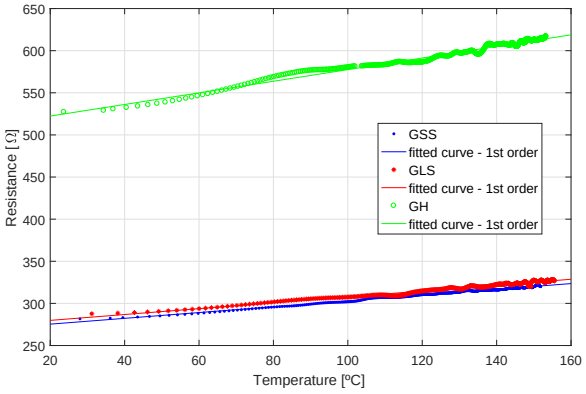


**Figure 9.** Relationship between the heater resistivity and the average chip temperature for the three heater chips. The sample heater chip used here presents a resistivity at room temperature of 520 Ω for GH, 276 Ω for GLS and 269 Ω for GSS.

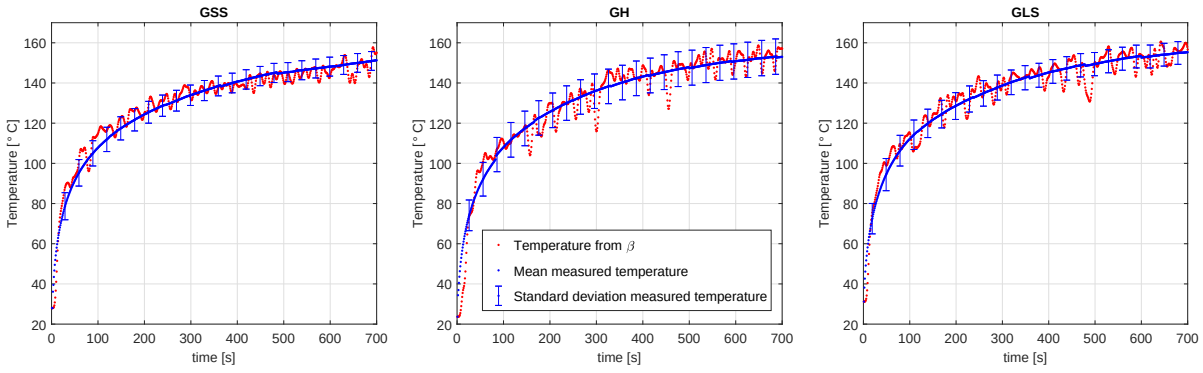


**Figure 10.** Comparison between the temperature measurement from the infrared camera and the calculated temperature based on Equation 7.

to the characterization of the devices/thrusters.

Figure 11 shows the relationship between the mass flow rate and the plenum pressure for different background pressure and different plenum temperature (room temperature and the temperature due to the heater chip temperature). An estimation of the plenum temperature can be done using the ideal gas equation. Assuming an isochoric process considering the same mass flow rate with different pressures, the gas temperature changes from the room temperature 24°C to 134.5°C. This temperature is close to the controlled chip temperature which is 149 ± 8°C. This difference is expected due to the heat transfer mechanism.

Figure 12 presents the thrust measurement as a function of the plenum pressures for different chip temperatures and background pressures. It shows the influence of the background pressure on the thrust level. The thrust tends to increase decreasing the background pressure meaning that in the space environment it expected a higher thrust.

Although higher chip temperatures appear at first sight to result higher thrust, this is not true since Figure 11 reveals that for the same mass flow rate the plenum pressure is different but the thrust is similar (see Figure 12). Similar conclusion can be drawn for the specific impulse looking at Figure 13. To analyse these results, two points have to be considered: there is a transition between the transitional regime and the continuum flow regime; the high temperature

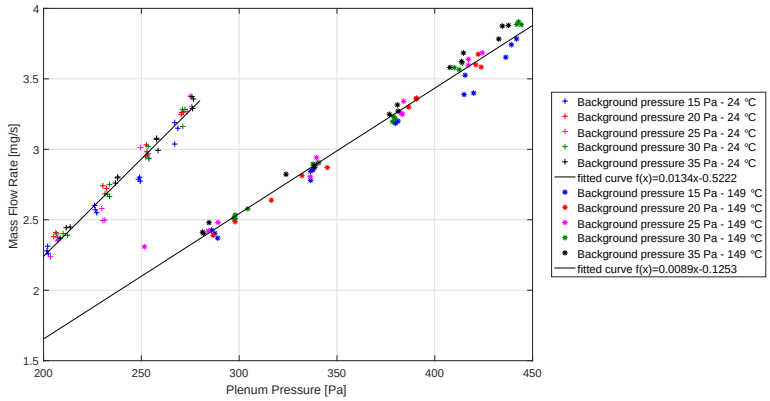


**Figure 11.** Relationship between the plenum pressure and the mass flow rate for different background pressures and different heater chip temperatures. The 1st order fitted curve present a R-square of 0.9663 for the room temperature 24°C and 0.9844 for the high temperature 149°C.

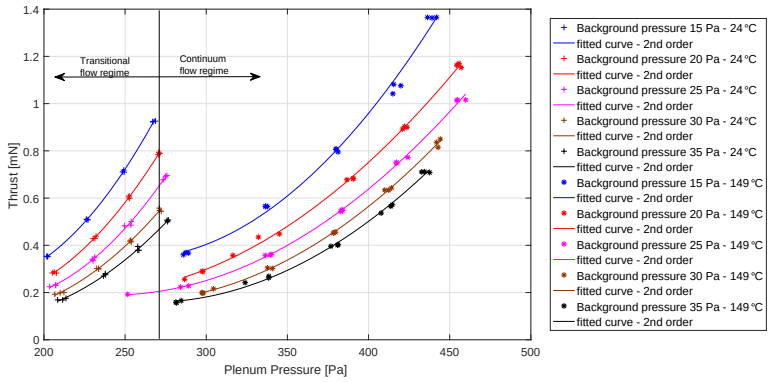


**Figure 12.** Relationship between the plenum pressure and the thrust for different background pressure and different heater chip temperature for GLS chip.

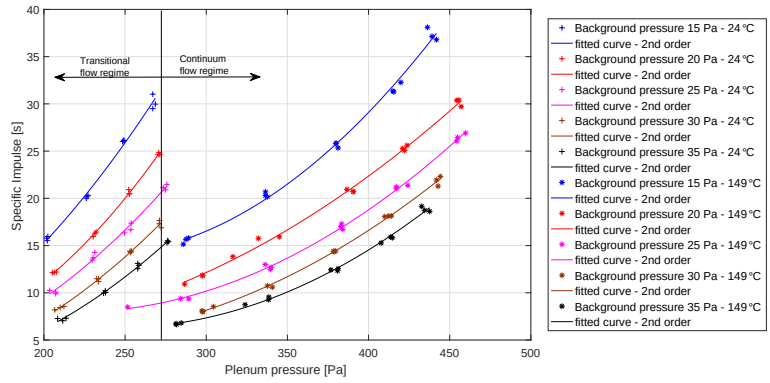


**Figure 13.** Relationship between the plenum pressure and the thrust for different background pressure and different heater chip temperature for GLS chip.

of the chip raises the temperature of the gas in the plenum, raising the plenum pressure.

The performance calculated from the equations 4 and 5 and using the experimental parameters result in thrust between 0.6 and 0.9 mN and specific impulse of 38 s for the room temperature experiment. For the high temperature experiment the thrust is between 0.9 and 1.4 mN and the specific impulse is 61 s. Although the Equations 4 and 5 are not applied for the continuum regime, it was calculated just to have a reference value.

Even though the tests were performed at non-ideal conditions, different than in the actual space environment, they are very useful for the development and characterization of the LPM. The background pressure is one of the main issues performing the tests, because it represents about 7.5% of the minimum plenum pressure, which was 200 Pa. Furthermore, the flow regime changes in the high temperature tests, and the corresponding increased plenum temperature is not a desired behaviour since it makes significantly more difficult to compare the results of tests conducted at different chip temperatures as the plenum pressure is also increased.

## 7. Conclusion

The design, manufacturing and characterization of a Low Pressure Micro-resistojet with an integrated heating and temperature sensing, was discussed. Three different designs were assessed in terms of their mechanical and electrical characterization. One design was used to assess the propulsion performance in near-operational conditions using Nitrogen as propellant. It was successfully demonstrated that this propulsion system has the potential for usage in very small satellites. Apart from its performance, it is inherent simplicity makes this design suitable for this class of satellites.

The manufacturing process was effective producing a total 48 devices with exception of two damaged. The two damaged devices were related to the GH chips, one the holes were not etched properly and another the Mo was not deposited correctly showing a discontinuity. In fact the GH wafer presented the highest electric resistivity as showed in the electric characterization. Generally speaking the deposition of the Mo was the main issue during the manufacturing process depositing lesser Mo than expected.

The mechanical and electrical characterization shows some differences between the designed and manufactured MEMS devices, but they were acceptable for the initial testing purposes. The Mo heater proved to be a good choice due to its stability at high temperatures up to 850°C allowing the measurement of the temperature as function of the resistivity. Due to that, the temperature was measured and controlled through the PID controller in a real time during the propulsion test. The propulsion characterization shows the potential of the thruster in a near-operational condition.

The special interface used to hold the heater chip was considered robust enough for the tests. However, for the next design and for the flight demonstration model, it is suggested to use a ceramic material instead of teflon. The use of ceramic material has some benefits such as much better isolation and resistance to very high temperature. The electric wires and components have to support high temperature since the heater chip is supposed to achieve temperatures up to 300°C, and in special cases even up to 600°C. This will require a careful re-design of the electrical path to the power supply.

Future research will be focused on four main aspects: to increase the heater chip temperature avoiding the increase of the plenum temperature; integrate electronics on the chip in order to have a better power control of the heaters; implement the usage of the water in a complete propulsion system; and, test the whole system in an actual-operational condition.

## Acknowledgments

The authors would like to express their sincere gratitude to the TU Delft Space Institute and the academic staff of the Space Systems Engineering chair of the Faculty of Aerospace Engineering

at TU Delft.

The research reported in this publication was supported by CNPq (Conselho Nacional de Desenvolvimento Científico e Tecnológico - Brasil), and CEFET-RJ (Centro Federal de Educação Tecnológica Celso Suckow da Fonseca do Rio de Janeiro).

## References

[1] Cervone A, Zandbergen B, Guerrieri D C, De Athayde Costa e Silva M, Krusharev I and van Zeijl H 2016 *CEAS Space Journal* 1–15 ISSN 1868-2510 URL http://dx.doi.org/10.1007/s12567-016-0135-3

[2] A Ketsdever, D Wadsworth, S Vargo, E Muntz 1998 AIAA/ASME/SAE/ASEE (34th AIAA/ASME/SAE/ASEE Joint Propulsion Conference and Exhibit)

[3] Ketsdever A D, Lee R H and Lilly T C 2005 *Journal of Micromechanics and Microengineering* **15** 2254 URL http://stacks.iop.org/0960-1317/15/i=12/a=007

[4] Palmer K, Nguyen H and Thornell G 2013 *Journal of Micromechanics and Microengineering* **23** 065006 URL http://stacks.iop.org/0960-1317/23/i=6/a=065006

[5] Cervone A, Mancas A and Zandbergen B 2015 *Acta Astronautica* **108** 30 – 39 ISSN 0094-5765 URL http://www.sciencedirect.com/science/article/pii/S0094576514005001

[6] Guerrieri D C, Cervone A and Gill E 2016 *Journal of Heat Transfer* **138** 112403 URL http://heattransfer.asmedigitalcollection.asme.org/article.aspx?articleid=2530390

[7] Guerrieri D C, Silva M A C, Cervone A and Gill E 2017 *Journal of Heat Transfer* **139** URL http://heattransfer.asmedigitalcollection.asme.org/article.aspx?articleID=2625789

[8] Mele L, Santagata F, Iervolino E, Mihailovic M, Rossi T, Tran A, Schellevis H, Creemer J and Sarro P 2012 *Sensors and Actuators A: Physical* **188** 173 – 180 ISSN 0924-4247 selected papers from The 16th International Conference on Solid-State Sensors, Actuators and Microsystems URL http://www.sciencedirect.com/science/article/pii/S0924424711006820

[9] J M Lafferty 1998 *Foundations of Vaccum Science and Technology* (John Wiley and Sons) ISBN 0-471-17593-5

[10] Bijster R J F 2014 *Design, Verification and Validation of a Micropropulsion Thrust Stand* Master thesis Delft University of Technology

[11] Jansen E H W 2016 *Improvement and validation of test stand performance for novel micropropulsion systems* Master thesis Delft University of Technology